Journal of Advanced Ceramics
先进陶瓷
ISSN 2226-4108
CN 10-1154/TQ
清华大学出版社 Tsinghua University Press
SciOpen

J Adv Ceram 2026, **15**: 9221362

https://doi.org/10.26599/JAC.2026.9221362

Research Article

A defect-chemical framework for transparent piezoelectric perovskites through donor-induced phase transitions

Su-Jin Ha[1], Young Kook Moon[1], Hyun-Ae Cha[1], Jong-Jin Choi[1,*], Byung-Dong Hahn[1,*], Byeong-Jae Min[2], Hyun-Cheol Song[2,*], Sahn Nahm[2], Seong-Hui Choi[3,4], Il-Ryeol Yoo[3], Kyung-Hoon Cho[3,4,*], Do-Cheon Ahn[5], Cheol-Woo Ahn[1,*]

[1]*Nano Materials Division, Korea Institute of Materials Science (KIMS), Gyeongnam 641-831, Republic of Korea*

[2]*Department of Materials Science and Engineering, Korea University, Seoul 02841, Republic of Korea*

[3]*School of Materials Science and Engineering, Kumoh National Institute of Technology, Gyeongbuk 39177, Republic of Korea*

[4]*Department of Energy Engineering Convergence, Kumoh National Institute of Technology, Gyeongbuk 39177, Republic of Korea*

[5]*Pohang Accelerator Laboratory, Pohang University of Science and Technology, Kyungbuk 37637, Republic of Korea*

*Corresponding authors:

E-mail: J.-J. Choi, finaljin@kims.re.kr;

B.-D. Hahn, cera72@kims.re.kr;

H.-C. Song, songhc@korea.ac.kr;

K.-H. Cho, khcho@kumoh.ac.kr;

C.-W. Ahn, cheoruahn@kims.re.kr

Received: June 8, 2026; Revised: August 24, 2026; Accepted: August 24, 2026

Abstract: Transparent piezoelectrics are often conceived as fundamentally distinct from conventional ferroelectric ceramics. However, this study reveals that transparency can be realized without altering the primary chemical framework, but rather through a strategically controlled donor-doping protocol. From an inorganic chemical perspective, this phenomenon is rooted in the defect chemistry of ABO_3 perovskites, where donor incorporation synergistically regulates charge compensation, lattice distortion, and interfacial sintering kinetics. Aliovalent donor doping induces cation-vacancy formation and attenuates local structural distortions, guiding ferroelectric lattices toward a pseudo-cubic state to suppress birefringence. Simultaneously, defect-mediated mass transport facilitates liquid-phase-mediated densification and regulates grain growth, eliminating scattering from residual porosity and grain boundaries. Consequently, optical transparency emerges as an intrinsic consequence of coupled defect equilibria, phase stability, and sintering dynamics. To validate the generalizability of this design concept, we systematically investigated representative donor-doped perovskite series, including Bi^{3+}-doped KNN and La^{3+}-doped PZT. Crucially, this study introduces a new paradigm that allows researchers to transform their established piezoelectric compositions into transparent multifunctional systems simply by incorporating donors, rather than abandoning proven materials for entirely new systems. Despite their distinct baseline structures, both systems exhibit a unified donor-induced transformation into transparent piezoelectric states. Our findings demonstrate that the transparent functionality can be integrated into existing piezoelectric systems through strategic modulation of defect equilibria and phase stability, providing a general defect-chemical framework for understanding and designing multifunctional transparent perovskite piezoelectrics. While this study focuses on

establishing the defect-chemical origin of transparency using total transmittance, detailed evaluations of haze and in-line transmittance for display and imaging applications are deferred to future study.

Keywords: Perovskite oxides, Donor doping, Defect chemistry, Polymorphic phase transition, Transparent piezoelectrics

1 Introduction

Since the seminal discovery of piezoelectricity by Pierre Curie and Jacques Curie in 1880 [1-3], perovskite ferroelectrics have emerged as one of the most intensively investigated classes of inorganic functional materials owing to their strong electromechanical coupling and exceptional compositional flexibility[4-12]. Among them, $Pb(Zr,Ti)O_3$ (PZT) and $(K,Na)NbO_3$ (KNN) represent prototypical ABO_3 systems in which crystallographic anisotropy, defect chemistry, and ferroelectric domain structures can be systematically engineered to optimize piezoelectric performance [13-21]. Despite decades of extensive compositional optimization, however, many conventional systems are now approaching their intrinsic performance limits, implying that further functional diversification requires fundamental inorganic chemical principles beyond empirical compositional tuning [22-25].

Transparent piezoelectrics have recently attracted considerable attention as multifunctional materials that simultaneously integrate optical transparency with ferroelectric functionality for applications in optoelectronics, sensing, energy harvesting, and bio-integrated devices [10,11,16-21,26-31]. As illustrated in Figs. 1 and S1, the realization of such systems requires both crystallographically oriented transparent particles (COTP, region 2) and fully dense transparent piezoelectric ceramics (TPC, region 3). Furthermore, Fig. S2 suggests that these functionalities can be achieved without fundamentally redesigning the parent compositions, implying that optical transparency is not restricted to a particular compositional family but rather emerges as a consequence of donor-controlled defect chemistry.

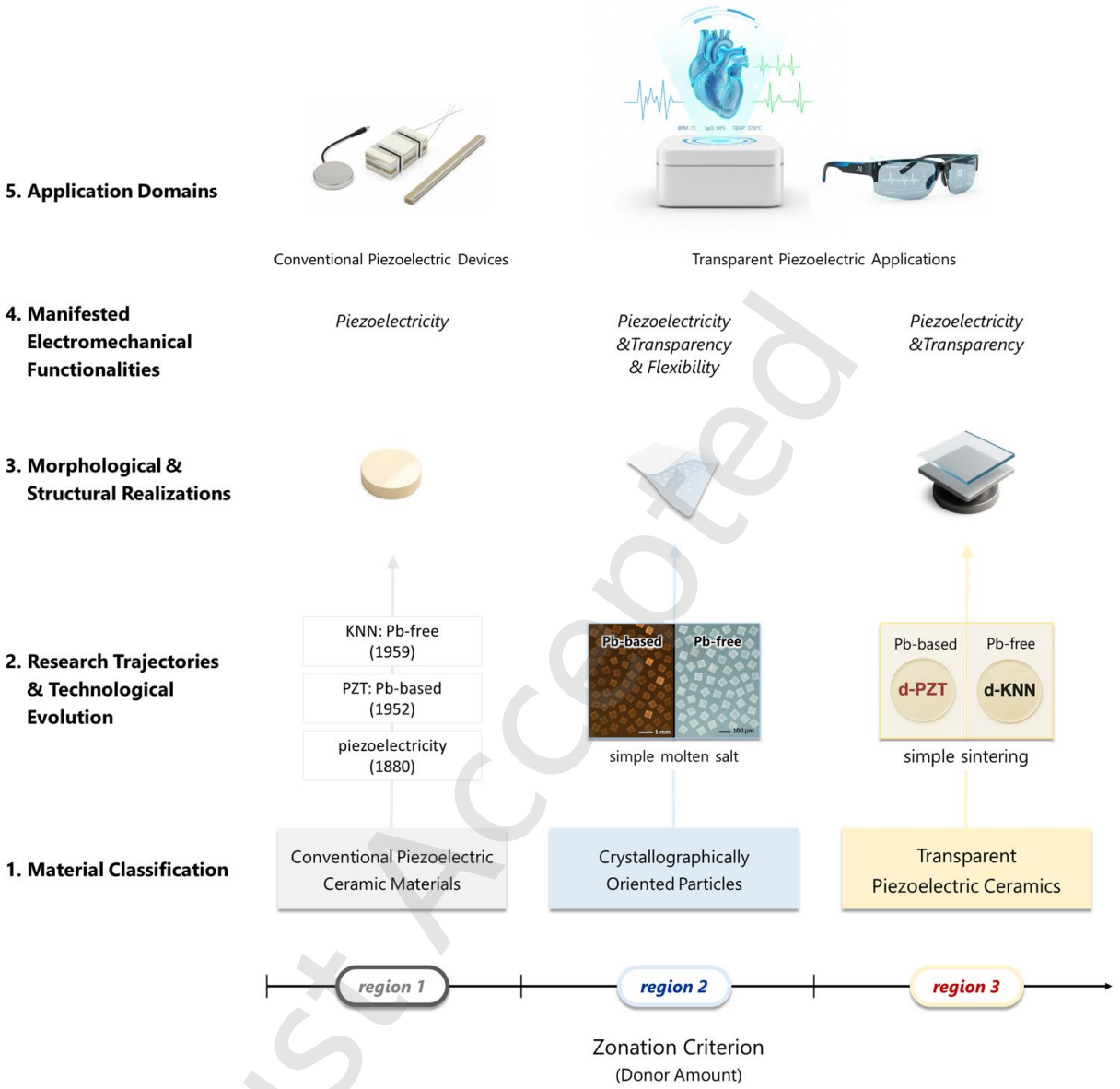

Fig. 1. Schematic diagram of multifunctional applications in transparent piezoelectric ceramic materials enabled by compositional design strategy based on donor doping.

Next-generation energy-harvesting devices, including smart lenses and glasses, haptic interfaces, and advanced biomedical systems such as holographic medical visualization, necessitate the prior development of "crystallographically oriented transparent particles (COTP, region 2)" and "transparent piezoelectric ceramics (TPC, region 3)". This study demonstrates that these materials can be fabricated in a straightforward manner by modulating the donor doping ratio while retaining conventional piezoelectric ceramic compositions. This figure includes elements generated using Gemini (Google) and DALL·E (GPT-4, OpenAI), based on descriptions provided by the authors.

From an inorganic chemical perspective, donor doping in ABO_3 lattices simultaneously regulates charge-compensation mechanisms, cation-vacancy equilibria, octahedral distortions, and sintering-related defect chemistry, which conceptually modifies the phase stability and transition behaviors of competing ferroelectric polymorphs [15,22,23,32-35]. This process systematically drives the crystallographic framework toward pseudo-cubic symmetry while also facilitating transient liquid-phase formation during high-temperature sintering, consequently enhancing densification and grain-growth kinetics [32,36,37]. Optical transparency therefore emerges not merely from densification itself, but from the coupled transition of phase stability, crystallographic isotropy, and interfacial mass transport.

A central yet previously underappreciated aspect of this mechanism is that, when interpreted consistently through the framework of inorganic chemistry, the origin of transparent piezoelectricity becomes conceptually straightforward, although it has historically been obscured by predominantly empirical compositional approaches. Importantly, the critical donor concentration is governed primarily by the intrinsic phase stability of the host lattice rather than by the specific chemical identity of the dopant, indicating a generalizable defect-chemical design concept across diverse perovskite systems.

To experimentally validate this framework, we deliberately selected representative compositional series in both KNN- and PZT-based systems and synthesized them under systematically controlled donor-doping conditions. Bi^{3+}-modified KNN and La^{3+}-modified PZT were chosen as model platforms because they are chemically distinct yet mechanistically complementary systems that enable systematic decoupling of defect chemistry, polymorphic phase transition, and densification behavior. In KNN-based systems, Bi^{3+} was specifically selected because its ionic radius (1.36 Å) is

comparable to those of the host alkali-site cations Na^+ (1.39 Å) and K^+ (1.64 Å), thereby enabling effective donor incorporation without inducing excessive lattice destabilization. In addition, Bi^{3+} has been extensively utilized as a donor species in the fabrication of transparent piezoelectric materials, making it both experimentally and technologically representative for validating the proposed framework [38-40]. By contrast, in PZT-based systems, La^{3+} was selected because donor dopants other than La^{3+} capable of producing transparent piezoelectric behavior have not yet been successfully established in this material system [41-44]. Across these experimentally fabricated compositions, we directly demonstrate that donor doping reproducibly induces optical transparency while preserving conventional piezoelectric compositions, thereby demonstrating that the proposed defect-chemical framework can describe transparency evolution in representative KNN- and PZT-based perovskite systems [45].

Overall, this study establishes donor doping as a general inorganic chemical design principle that fundamentally links defect thermodynamics, polymorphic phase transitions, and sintering kinetics. By experimentally synthesizing and transparently converting the representative material systems introduced above, we directly validate the proposed theoretical framework and demonstrate that transparent piezoelectricity can emerge as a general consequence of donor-controlled polymorphic phase transitions in conventional perovskite ceramics.

2. Experimental

"$(K_{0.5}Na_{0.5})NbO_3$ (KNN) + x at.% Bi_2O_3" (x=0.0-5.0), "0.975KNN-0.025$(Na,Bi)TiO_3$ (KNN-NBT)+ x at.% Bi_2O_3" (x=0.0-6.0), "$(K,Na,Ba)NbO_3$ (KNBN) + x at.% Bi_2O_3" (x=0.0-6.0), and "$(K,Na)(Nb,Sb)O_3$-$CaZrO_3$ (KNNS-CZ) + x at.% Bi_2O_3" (x=0.0-2.0) ceramics were synthesized through conventional solid-state reaction method. The high-purity powder of K_2CO_3, Na_2CO_3, Nb_2O_5, Sb_2O_3, Bi_2O_3, $CaCO_3$, $BaCO_3$, ZrO_2, TiO_2 (≥ 99.9%, Sigma-Aldrich) were mixed in a

polypropylene jar with zirconia balls for 24 h. The slurry was dried at 80℃ and then calcined at 850-900℃ for 3 h. The calcined powders were subsequently milled for 24 h, dried and uniaxially pressed into pellets under pressure of 100 MPa. The green pellets were sintered at temperatures ranging from 1020-1180℃ for 2-10 h. A heating rate of 5 ℃/min was applied, and the samples were furnace-cooled to room temperature. Single-crystal specimens derived from diverse compositions, including KNN + Ba^{2+}, KNN + Ca^{2+}, KNLN + Ba^{2+}, and Mn-KNN-LS + Bi^{3+} systems, were fabricated via conventional ceramic sintering routes. All samples were processed within a sintering temperature window of 1050-1100°C.

"$(Pb_{1-x}La_x)(Zr,Ti)O_3$ (PLZT, x=8.4-9.0, PZT + x at.% La_2O_3)" ceramic were synthesized through conventional solid-state reaction method. PbO, La_2O_3, TiO_2 (99.9%, Sigma-Aldrich), and ZrO_2 (99%, Kanto Chemical) were used. The mixtures were ball-milled in a polypropylene jar with zirconia balls for 24 h. After milling, the slurry was dried and calcined at 900℃ for 2 h. The calcined powders were milled for 48 h, dried and then compacted into pellets through cold isostatic pressing (CIP) at 200 MPa for 5 min. The green pellets were sintered at 1200℃ for 8 h in an oxygen atmosphere.

2.1. Analyses of Microstructure and Crystal Structure

The crystal structures of sintered specimens were characterized using the patterns of X-ray diffraction (XRD, Rigaku, D/max-500VL/PC) with Cu Kα radiation (λ=0.1542 nm). The microstructures were observed using scanning electron microscope (SEM, JSM-6610LV;JEOL Ltd., Japan). The microstructure and elemental distribution of the KNN ceramic were examined using transmission electron microscopy (TEM, JEM-2100F; JEOL Ltd., Japan).

2.2. Property Measurement

The sintered specimens were mirror-polished to a thickness of 0.5-1.0 mm using 1.0 μm diamond slurry. The bulk densities (ρ) of the specimens were measured by the Archimedes method using m-xylene as the immersion medium. The samples were poled in silicone oil at 120℃ by applying a DC electric field of 4.0-5.0 kV/mm for 30 min and conducted to age for 24 h prior to electrical characterization. The piezoelectric constant (d_{33}) was measured using a d_{33} meter (Product DT-3300, Micro-Epsilon Channel), while dielectric properties and impedance spectra were recorded using an impedance analyzer (4294A, Agilent Technologies, Santa Clara, CA, USA). The polarization-electric field (P-E) hysteresis loops were obtained using a standard test system (Precision LC-II, Radiant Technologies, USA). Temperature-dependent dielectric constant and loss tangent were measured using an LCR meter (HP 4284A) coupled with a programmable temperature-controlled furnace (Delta 9023). The optical transmittance spectra were recorded from 200 to 1400 nm using a UV-Vis spectrometer (Carry 5000, Agilent Technologies, USA).

3. Result and discussion

3.1. Donor-Induced Structural Transitions and Liquid-Phase Densification in Perovskite Piezoceramics

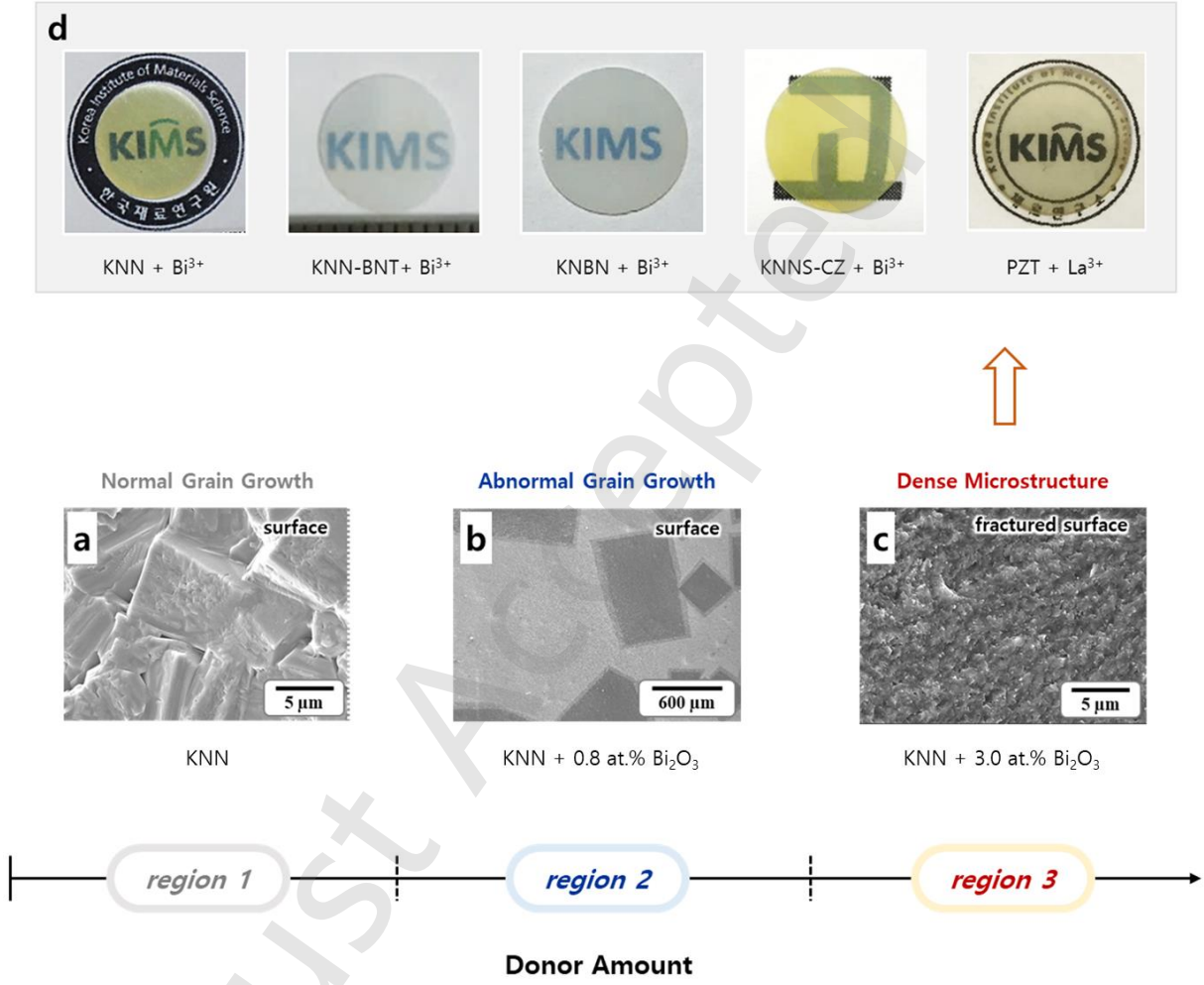

Fig. 2. Conversion of conventional piezoelectric ceramics into single-crystalline and optically transparent materials via donor doping (sample thickness of KNN: 0.5 mm, sample thickness of PLZT: 1.0 mm)**.**

a-c, SEM (SE) micrographs of KNN ceramics with varying Bi^{3+} doping concentrations: (a) undoped KNN, (b) KNN + 0.8 at.% Bi_2O_3, and (c) KNN + 3.0 at.% Bi_2O_3.

d, Optical images of optically transparent ceramics obtained through donor doping in KNNs and PZT. The faint yellow hue occasionally observed in some specimens is generally attributed to defect-related visible-light absorption and associated color-center formation; however, the origin of this coloration was not investigated in this study.

PZT has long served as the prototypical piezoelectric perovskite because of its exceptional electromechanical coupling and broad compositional tunability, whereas KNN-based systems have emerged as representative lead-free alternatives driven by environmental and regulatory considerations [46,47]. Despite decades of compositional optimization, however, the development of both systems has remained largely confined to conventional opaque polycrystalline ceramics corresponding to region 1 in Figs. 1-2 and S3 [32]. In most previous studies, donor incorporation was primarily employed as an empirical strategy for tuning dielectric and piezoelectric properties. Although substantial advances have been achieved in these functional aspects, the inorganic chemical principles governing transparency in donor-modified piezoelectric ceramics remain insufficiently understood, particularly regarding the coupled interplay among aliovalent substitution, crystallographic phase transitions, defect equilibria, and liquid-phase-assisted interfacial densification.

In the present study, donor incorporation for the realization of transparent piezoelectric ceramics is identified as a chemically active parameter that simultaneously governs crystallographic symmetry, defect-mediated phase stability, grain-growth behavior, and densification pathways in perovskite lattices. As summarized in Figs. 2 and S3-S4, increasing donor concentration induces a sequential transformation from conventional polycrystalline ceramics to crystallographically coherent transparent domains and ultimately to optically transparent dense ceramics. These donor-induced transparency regimes can be systematically classified into three distinct functional categories according to the donor concentration and the corresponding structural response of the host lattice.

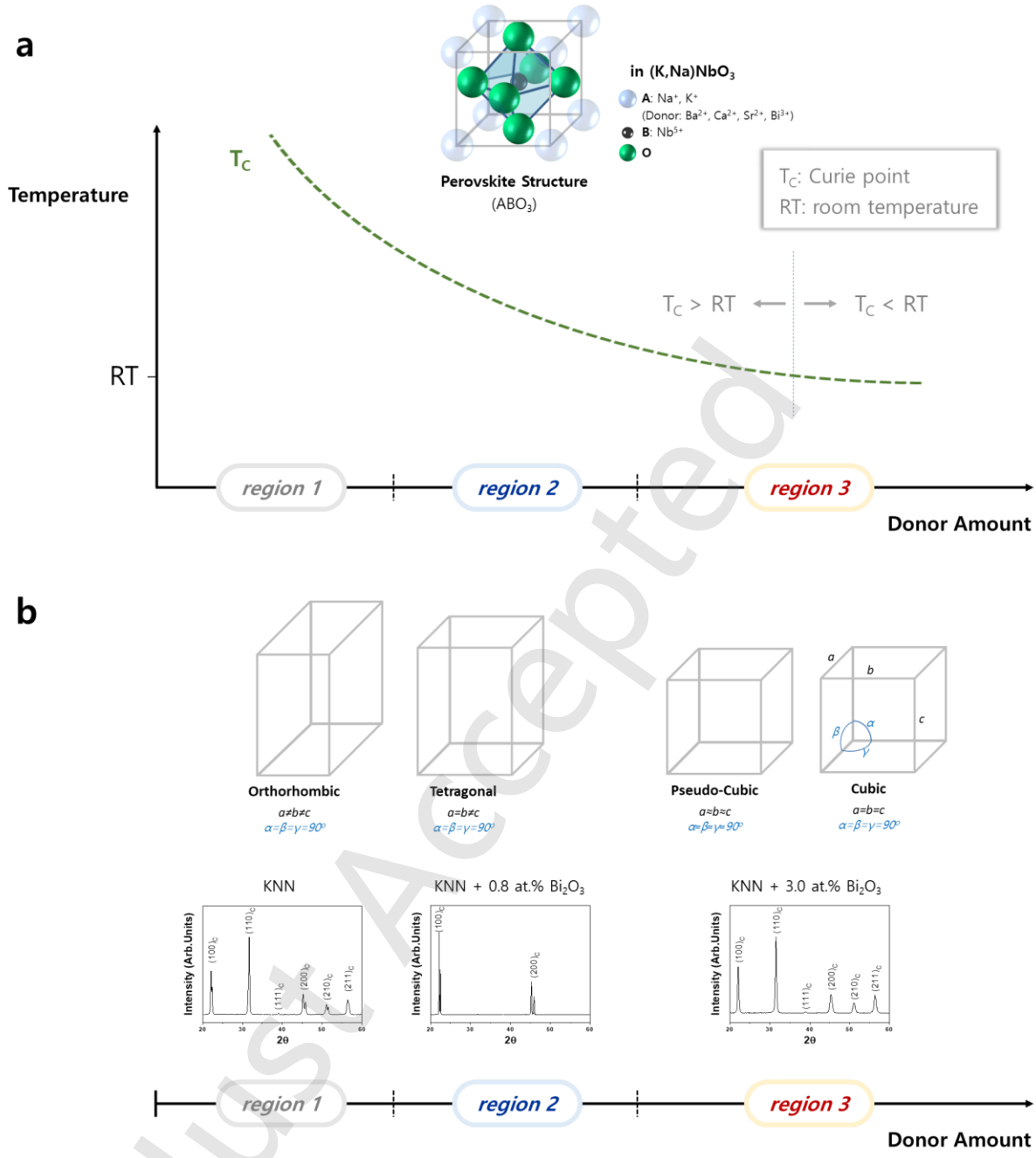

Fig. 3. Donor-modulated polymorphic phase transition and symmetry modulation in KNN perovskite ferroelectrics.

a, Variation of Curie temperature (T_C) with donor concentration, indicating compositional control of ferroelectric stability via defect-mediated lattice modification.

b, Donor-induced polymorphic phase transition across rhombohedral (R), orthorhombic (O), tetragonal (T), pseudo-cubic (PC), and cubic (C) phases, together with representative XRD patterns from selected specimens in Regions 1-3, showing progressive symmetry enhancement and reduced structural anisotropy, thereby reflecting defect-lattice coupling in KNN perovskites.

The SEM (SE) micrographs shown in Figs. 2a-c and S3-S4 demonstrate that Bi^{3+} incorporation significantly modifies the grain-growth behavior of KNN ceramics. At low donor concentrations, the microstructure consists of relatively fine equiaxed grains characteristic of conventional solid-state sintering, whereas increasing donor concentration induces pronounced grain coarsening and the formation of crystallographically coherent domains. From an inorganic chemical perspective, this behavior originates from coupled interactions among aliovalent substitution, defect equilibria, and thermodynamically activated alkali volatilization in KNN-based systems, which progressively promote localized liquid-phase formation and enhance interfacial transport kinetics during sintering [46,47]. Within region 2, these liquid-phase-assisted processes induce abnormal grain growth (AGG) and the formation of large crystallographically coherent domains. The detailed mechanism of AGG-driven single-crystal-like growth has been comprehensively discussed in the previous literature [32]. Upon further donor incorporation, however, AGG becomes progressively suppressed, and region 3 evolves into a highly dense fine-grained microstructure with minimal residual porosity.

KNN-based ceramics exhibit partial melting behavior near 1200°C, as shown in Fig. S5. Therefore, when sintering is performed at temperatures slightly below the melting point under conditions suppressing excessive alkali volatilization, sufficient liquid phases can be generated without catastrophic structural collapse. Under these conditions, residual pores are efficiently eliminated through liquid-phase-assisted densification, enabling relative densities exceeding 99.9%, which are essential for achieving optical transparency in polycrystalline ceramics. Although the relative density cannot be strictly defined by a universal threshold of 99.9%, all specimens exhibiting high optical transparency in the present study consistently showed highly dense microstructures with relative densities exceeding 99.9%.

Simultaneously, donor incorporation induces pronounced polymorphic phase transitions within the perovskite framework. As shown in Fig. 3, increasing donor concentration systematically shifts the phase constitution toward higher-symmetry structural states accompanied by progressive suppression of long-range ferroic distortion. Such behavior reflects donor-induced destabilization of symmetry-lowered ferroelectric polymorphs through modification of local lattice energetics and crystallographic anisotropy.

In ABO_3 perovskites, the relative stability of rhombohedral, orthorhombic, tetragonal, and pseudo-cubic polymorphs is governed by subtle differences in octahedral distortion energetics, ionic displacement behavior, and lattice anisotropy. Because ferroelectricity in KNN-based systems originates from cooperative ionic displacement and anisotropic BO_6 octahedral distortion, aliovalent substitution at the A-site can strongly perturb the energetic balance among competing ferroic states. Donor incorporation modifies local electrostatic interactions, alters cation-vacancy equilibria, and weakens the directional lattice distortion necessary for stabilization of symmetry-lowered ferroelectric phases. As a consequence, increasing donor concentration progressively destabilizes orthorhombic and tetragonal ferroic order and promotes pseudo-cubic structural characteristics associated with reduced lattice anisotropy and suppressed birefringence.

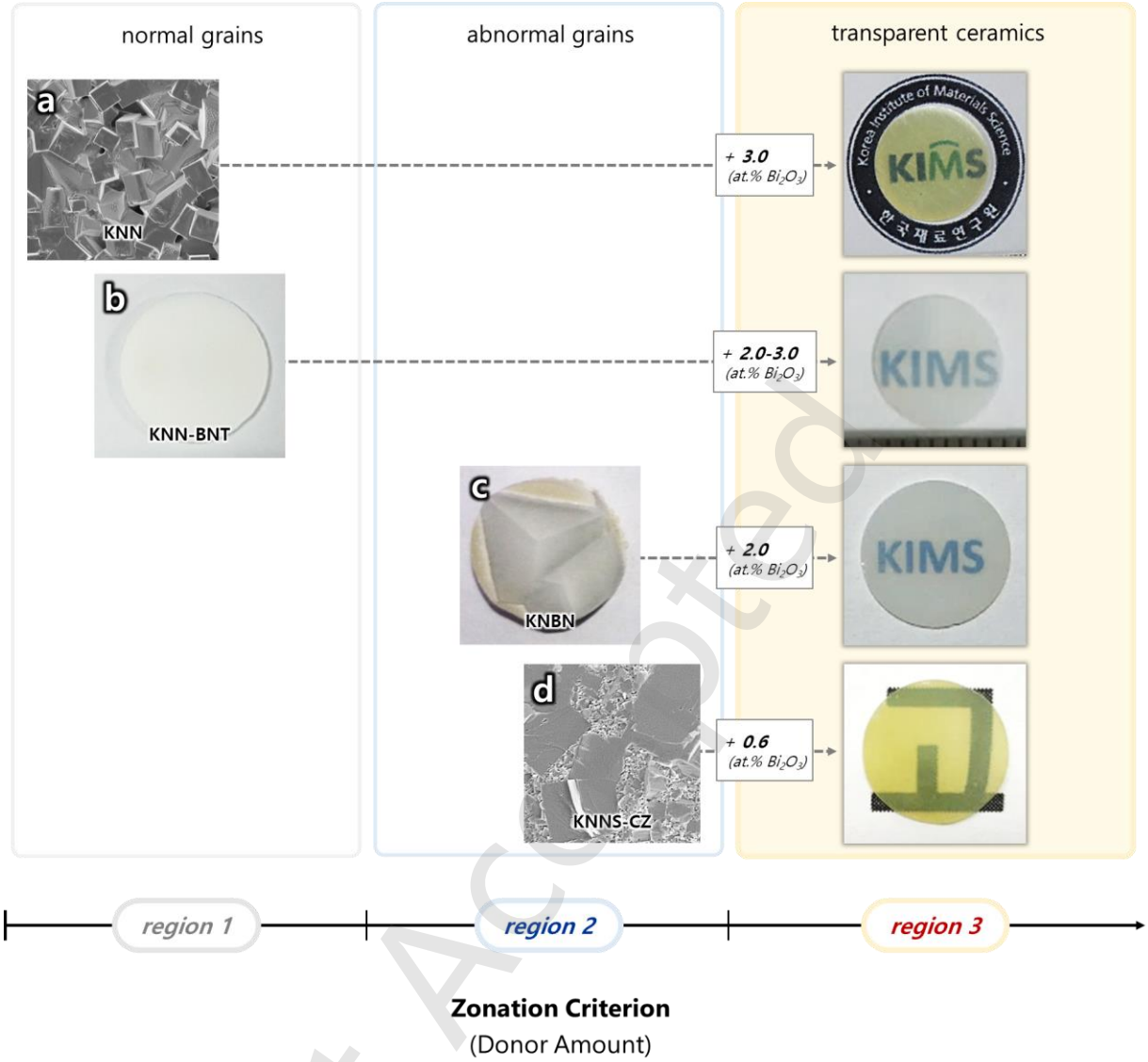

Fig. 4. Composition-dependent donor concentrations required for pseudo-cubic stabilization in KNN-based perovskites (sample thickness: 0.5 mm)**.**
a, KNN + 3.0 at.% Bi_2O_3; **b**, 0.975KNN-0.025(Bi,Na)TiO_3 (KNN-BNT) + 2.0-3.0 at.% Bi_2O_3; **c**, KNBN + 2.0 at.% Bi_2O_3; **d**, (K,Na)(Nb,Sb)O_3-$CaZrO_3$ (KNNS-CZ) + 0.6 at.% Bi_2O_3. The results demonstrate that the donor concentration required to induce pseudo-cubic stabilization varies systematically with the initial polymorphic energy landscape of each KNN-based composition.

Importantly, Fig. 4 further demonstrates that the critical donor concentration required for pseudo-cubic stabilization strongly depends on the intrinsic crystallographic location of the host composition within the polymorphic phase landscape. Compositions positioned near polymorphic phase boundaries already possess relatively shallow free-energy differences among competing structural states and

therefore exhibit intrinsically weakened ferroic anisotropy. In these systems, only a small degree of donor-induced perturbation is sufficient to destabilize long-range ferroic order and induce a transition toward a pseudo-cubic structure. By contrast, compositions located deep within structurally stable orthorhombic or tetragonal regions possess substantially larger energetic barriers against symmetry elevation and therefore require significantly greater donor incorporation to induce comparable crystallographic transitions.

This compositional dependence is consistently observed across multiple KNN-based solid-solution systems in Fig. 4. Systems positioned near rhombohedral-orthorhombic or orthorhombic-tetragonal polymorphic boundaries exhibit rapid symmetry transition even at relatively low donor concentrations, whereas compositions with robust ferroic distortion retain anisotropic structural characteristics over a substantially broader compositional range. These observations indicate that donor-induced pseudo-cubic stabilization is fundamentally governed by the intrinsic phase stability and lattice susceptibility of the host composition rather than by the specific chemical identity of the donor species itself.

Moreover, the structural transformation observed here should not be interpreted as a simple transition toward an ideal nonpolar cubic phase. Instead, the pseudo-cubic state appears to involve progressive disruption of long-range ferroic coherence while preserving local polar heterogeneity at shorter length scales. Such structurally heterogeneous states are consistent with the diffuse crystallographic characteristics commonly observed in donor-modified perovskite systems and are particularly important for simultaneously suppressing optical scattering while retaining functional electromechanical responses.

Accordingly, Figs. 3-4 collectively establish that donor incorporation functions not merely as an empirical compositional modifier, but as a chemically active parameter capable of systematically

regulating defect chemistry, crystallographic phase stability, ferroic anisotropy, and interfacial kinetic behavior in conventional piezoelectric perovskites. These results demonstrate that optical transparency emerges through donor-mediated destabilization of long-range ferroic order combined with -liquid-phase-assisted densification, thereby providing a chemically generalizable framework for transforming conventional piezoelectric ceramics into multifunctional transparent materials.

3.2. Donor-driven crystallography and liquid-phase densification in transparent perovskites

Donor concentration strongly modifies densification behavior through its influence on liquid-phase formation during sintering. KNN-based systems exhibit melting behavior near approximately 1200°C, as shown in Fig. S5. Accordingly, when sintering is conducted slightly below the melting temperature, typically within 1160-1180°C, substantial intergranular liquid formation can occur while preserving the overall ceramic framework. In KNN ceramics, this liquid phase is generally understood to originate from preferential Na volatilization during sintering, which locally produces a K-rich liquid phase [22]. Donor addition further accelerates Na volatilization, thereby promoting liquid-phase formation [32]. TEM observations (Fig. S6) provide direct evidence for this liquid-phase-assisted densification mechanism. As shown in Fig. S6a, the ceramic exhibits a highly dense microstructure with negligible residual porosity. The TEM image (Fig. S6b) reveals that the Bi-containing intergranular phase is preferentially distributed at triple grain junctions (TGJs) and along grain boundaries (GBs), while a detectable amount of Bi also remains within the grain interiors (GIs). Furthermore, the EDS line scan across the TGJ (Fig. S6c) demonstrates pronounced enrichment of both Bi and K within the intergranular phase. Considering that liquid formation in KNN originates from Na volatilization and that Bi further enhances this volatilization [22,32], the observed K- and Bi-rich intergranular phase is considered to represent the retained liquid phase formed during sintering.

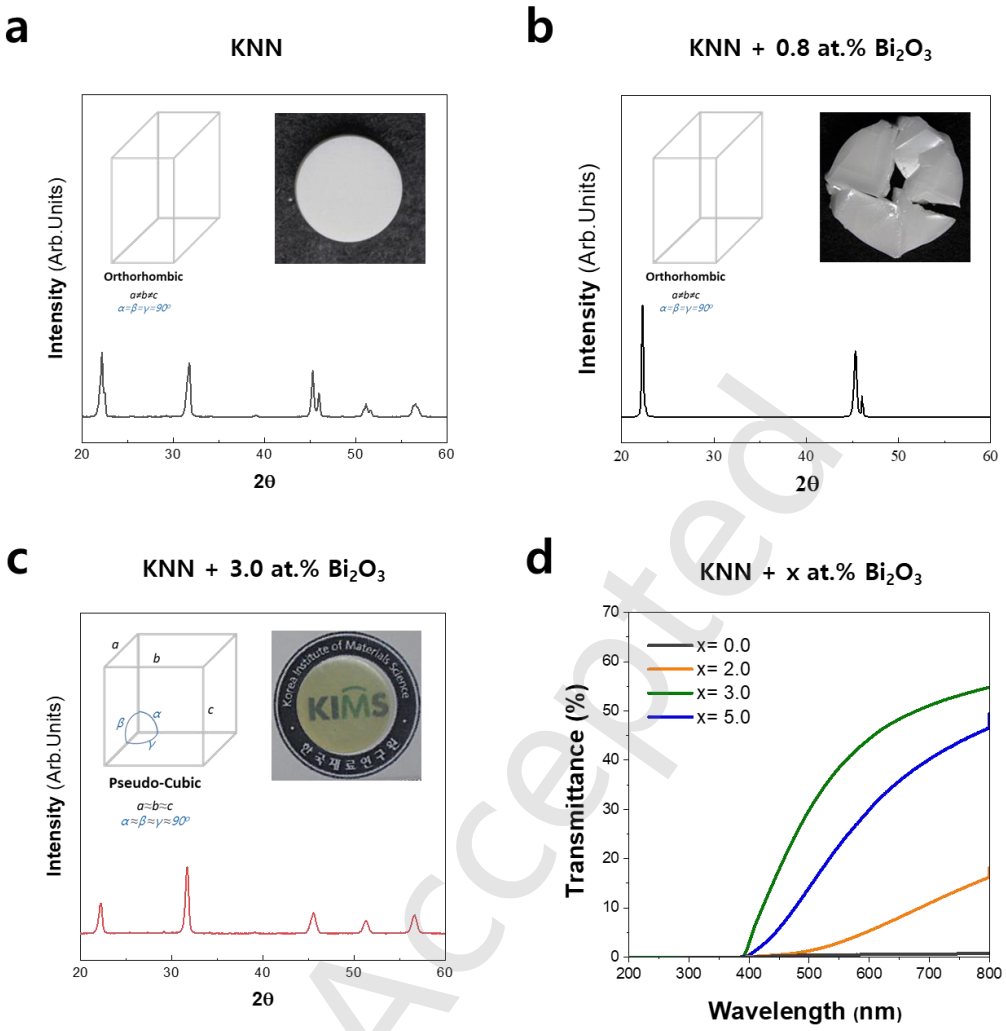

Fig. 5. Optical appearance and structural transition in KNN + x at.% Bi_2O_3 ceramics. a-c, Photographic images representing distinct structural and growth regimes: **a**, region 1, a conventional opaque polycrystalline state; **b**, region 2, characterized by abnormal grain growth (AGG) leading to large-scale single-crystalline domains; and **c**, region 3, highly transparent state (sample thickness: 0.5 mm). The transition to region 3 is fundamentally driven by a structural shift toward pseudo-cubic symmetry. This phase transition, in conjunction with high densification, eliminates birefringence-induced light scattering while preserving the piezoelectric properties of the KNN matrix. **d**, Comparative visual transparency and optical quality across various Bi^{3+}-doped perovskite systems. The stabilization of the pseudo-cubic phase effectively bypasses the inherent optical limitations of traditional anisotropic perovskite structures, enabling the realization of high-performance transparent piezoelectric ceramics.

The liquid phase plays a direct structural role in eliminating residual porosity and stabilizing an ultimately dense microstructure. The preferential accumulation of this retained liquid phase at TGJs and along GBs facilitates the filling of residual intergranular pores and capillary channels, thereby eliminating internal voids that would otherwise remain as strong optical scattering centers. Consequently, the transparent specimens achieve relative densities exceeding 99.9%, effectively suppressing porosity-induced light scattering. The retained intergranular liquid phase is therefore intrinsically associated with the optical transparency of the final ceramic body.

In addition to the liquid-phase-assisted densification described above, donor-induced crystallographic transition provides the second fundamental mechanism responsible for transparency in perovskite piezoelectric ceramics. As demonstrated in Fig. 4, different compositional systems require substantially different donor concentrations to induce pseudo-cubic stabilization depending on their intrinsic crystallographic phase stability. Accordingly, Figs. 5-7 and Figs. S7-S18 examine these representative systems in detail, elucidating how donor incorporation systematically transforms conventional opaque ceramics into highly transparent piezoelectric oxides through coupled modifications of phase stability, defect chemistry, and sintering kinetics.

X-ray diffraction effectively captures structural transitions in KNN-based systems, as the orthorhombic distortion within the parent lattice generates clearly distinguishable diffraction peaks. As shown in Figs. 5a-c, pristine KNN exhibits characteristic orthorhombic peak splitting associated with anisotropic ferroic lattice distortion. Upon donor incorporation, these diffraction features progressively merge, indicating systematic suppression of crystallographic anisotropy and destabilization of the orthorhombic phase. Beyond a critical donor concentration, nearly indistinguishable diffraction profiles emerge, consistent with the stabilization of a pseudo-cubic structural state.

From an inorganic chemical perspective, this behavior originates from aliovalent substitution within the ABO_3 framework and the accompanying modification of local defect equilibria. Donor incorporation perturbs charge neutrality, increases cation-vacancy concentration, and modifies the local bonding environment surrounding the BO_6 octahedra. These local structural perturbations progressively destabilize the cooperative ionic displacements responsible for ferroic distortion. As the donor concentration increases, the free-energy difference between competing polymorphs decreases, driving the lattice toward crystallographic states with reduced spontaneous strain and lower structural anisotropy.

The suppression of optical scattering caused by birefringence is primarily driven by the donor-induced shift toward a pseudo-cubic structure. In polycrystalline ferroelectrics, anisotropic ferroic distortion generates local refractive-index variations between neighboring grains, resulting in severe light scattering. Therefore, progressive reduction of crystallographic anisotropy through donor-induced symmetry transition is essential for achieving optical transparency.

To further clarify the relationship between the average and local crystal structures, synchrotron XRD Rietveld refinement and TEM-EDS elemental mapping were performed, as shown in Figs. S7 and S8. The coexistence of one tetragonal and two cubic phases revealed by synchrotron XRD Rietveld refinement is attributed to grain-scale compositional heterogeneity arising from the non-uniform distribution of K, Na, and Bi. TEM-EDS elemental mapping further confirms grain-to-grain compositional heterogeneity, showing variations in the K/Na ratio among neighboring grains and a slight tendency for Bi to be enriched in K-rich grains. Such local chemical heterogeneity is expected to produce locally different structural stabilities, resulting in an average crystal structure that is best described by a multiphase model rather than a single cubic phase. Specifically, grain-scale

fluctuations in Bi concentration dictate these local structural variations. Grains with a higher local Bi content are structurally driven toward a highly symmetric cubic-like state, whereas grains with lower Bi concentration tend to retain the anisotropic tetragonal (T) symmetry. Consequently, the macroscopically observed pseudo-cubic phase does not represent a perfectly uniform single-phase state but is rather an average structural manifestation of these local compositional and symmetry fluctuations. While the presence of polar nanoregions (PNRs) cannot be completely ruled out, the current experimental evidence primarily supports grain-scale compositional heterogeneity as the origin of the observed structural complexity.

Taken together, optical transparency in these systems originates from the simultaneous suppression of two fundamentally different scattering sources: crystallographic scattering arising from ferroic anisotropy and microstructural scattering originating from residual porosity. The former is suppressed through donor-induced pseudo-cubic stabilization, whereas the latter is eliminated through liquid-phase-assisted densification driven by enhanced Na volatilization during sintering. The coupled operation of these two mechanisms enables highly transparent polycrystalline piezoelectric ceramics, as evidenced by the optical characteristics shown in Figs. 5 and S9.

It should be noted that the optical transmittance reported in the present study corresponds to the total transmittance, which reflects the overall suppression of optical scattering arising from donor-induced densification and reduced birefringence. In contrast, direct (in-line) transmittance and haze provide additional information regarding forward light scattering and image clarity, which are particularly important for imaging and display applications. Therefore, although the high total transmittance observed here demonstrates the successful realization of transparent piezoelectric ceramics, it does not necessarily imply the complete elimination of forward scattering. Residual grain-boundary heterogeneity, local compositional fluctuations, and refractive-index variations may still contribute to

haze. A comprehensive evaluation of imaging quality through haze and in-line transmittance measurements will therefore be an important subject of future studies.

The abnormal grain growth behavior observed in region 2 is mechanistically distinct from the transparency mechanism established in region 3. In region 2, liquid-phase-assisted grain-boundary migration promotes the formation of large crystallographically coherent domains with reduced internal scattering, thereby producing transparent single-crystal-like particles. Because the detailed kinetic mechanism governing this abnormal grain growth behavior has already been comprehensively reported in the previous literature [32], only representative results are briefly presented here together with Figs. S3-S4.

The generality of donor-mediated crystallographic destabilization is further demonstrated across multiple KNN-based solid-solution systems summarized in Figs. 6, 7, and S10-S13. Although solid-solution formation itself influences phase stability through lattice accommodation effects, the present results reveal that donor incorporation exerts the dominant influence on symmetry transition. In particular, donor doping systematically drives the lattice toward pseudo-cubic symmetry even in compositions initially located within multiphase ferroelectric regimes.

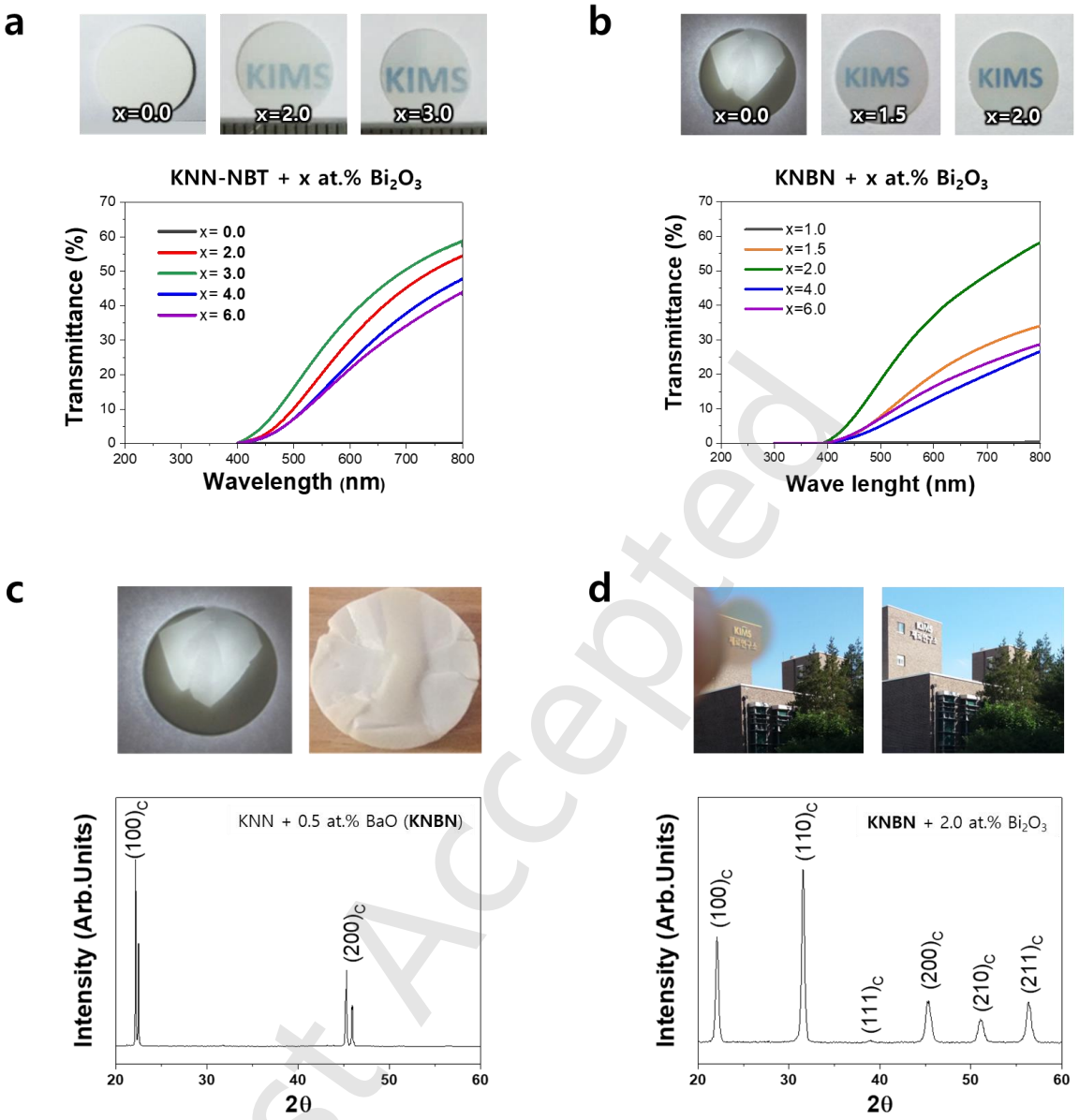

Fig. 6. Compositional dependence of structural and optical behaviors in KNN-based solid solutions as a function of Bi^{3+} content. a-b, Photographic images and wavelength-dependent transmittance of **a** KNN-NBT and (b) KNBN systems (sample thickness: 0.5 mm). The pristine samples initiate from an opaque polycrystalline state (**region 1**), transitioning toward transparency with increasing Bi^{3+} content. **c-d,** XRD patterns and corresponding specimen photographs illustrating the shift in growth and structural regimes: (c) **region 2** of pristine KNBN, characterized by opacity due to abnormal grain growth and single-crystalline domain formation, and (d) **region 3** of Bi^{3+}-doped KNBN. The **structural shift** from region 2 to region 3 is fundamentally driven by a transition toward pseudo-cubic symmetry; this transformation eliminates birefringence-induced light scattering, thereby enabling the development of high-performance transparent piezoelectric ceramics.

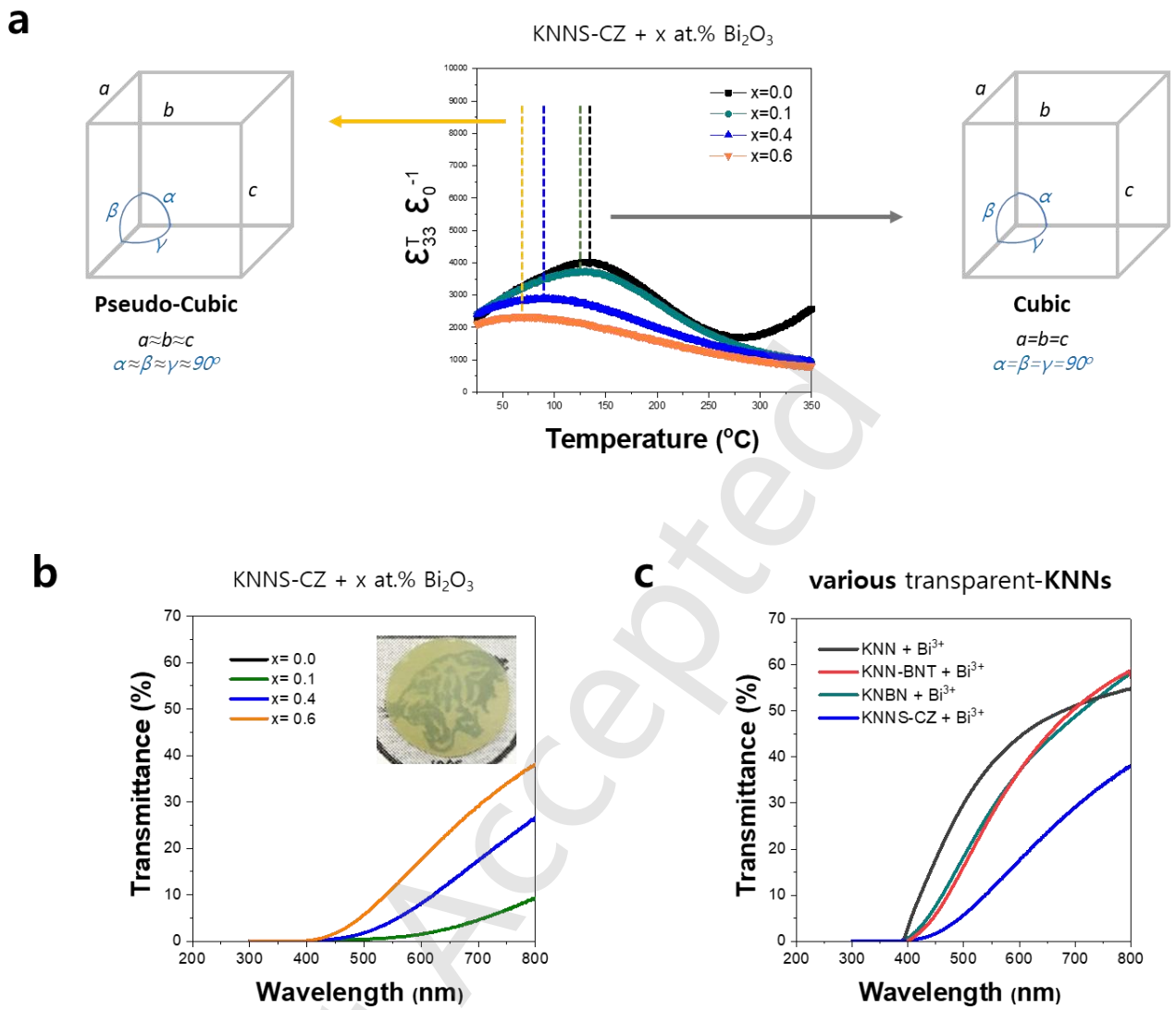

Fig. 7. Dielectric and optical characterization of KNNS-CZ + x at.% at.% Bi_2O_3 **and various KNN-based transparent systems** (sample thickness: 0.5 mm)**. a**, Temperature-dependent dielectric permittivity Bi^{3+}-doped KNNS-CZ ceramics. The progressive shift in the Curie temperature (T_C) serves as a primary indicator of the structural transition toward pseudo-cubic symmetry, a modification that is subtle and difficult to resolve via conventional XRD. **b**, Corresponding optical transmittance spectra and photographic images of the KNNS-CZ specimens, demonstrating the transition from an opaque state to high transparency as a function of Bi^{3+} content. **c**, Comparative optical transmittance of various KNN-based solid solutions investigated in this study.

For certain systems, the structural transformation can be unambiguously characterized through diffraction analysis alone, as the reduction in symmetry induces distinct and resolvable peak

splitting. However, in compositions exhibiting diffuse structural heterogeneity or broadened diffraction features, XRD alone becomes insufficient for rigorous structural interpretation. This limitation is particularly evident in the KNNS-CZ system shown in Fig. 7 and Fig. S11, where diffraction broadening obscures the precise structural transition pathway.

Accordingly, temperature-dependent dielectric permittivity analysis was additionally employed to resolve donor-induced phase transition in such systems. As shown in Figs. 7a and S15, systematic shifts in dielectric anomalies and progressive broadening of phase-transition behavior reveal gradual destabilization of long-range ferroic ordering with increasing donor concentration. These results demonstrate that structural transitions mediated by donors in chemically complex perovskites often elude rigorous interpretation via diffraction analysis alone, necessitating complementary thermodynamic and dielectric characterization.

The KNNS-CZ system provides a representative example of the critical role of liquid-phase-assisted densification in achieving optical transparency. As shown in Fig. S16, KNNS-CZ ceramics containing 0.6 at.% Bi_2O_3 exhibit markedly different microstructures depending on the sintering temperature. At 1160 °C, the amount of liquid phase is insufficient to completely eliminate intergranular pores, resulting in a relatively low relative density of 92.5% and an opaque appearance. In contrast, sintering at 1180 °C generates sufficient liquid phase to fill the residual pores and achieve nearly complete densification, yielding a relative density of 99.9%. After polishing, the highly densified specimen exhibits optical transparency.

Despite the successful realization of optical transparency, KNN-based systems exhibit intrinsic limitations in simultaneously maintaining high piezoelectric activity. As shown in Fig. S17, the KNNS-CZ composition initially exhibits piezoelectric coefficients exceeding 300 pC N^{-1} in the

conventional opaque state; however, transformation into the transparent pseudo-cubic regime reduces the piezoelectric response to below 100 pC N^{-1}. This degradation originates from the combined effects of donor-induced grain refinement and progressive suppression of ferroic anisotropy. Although a detailed quantitative correlation between the specific donor concentration, fine structural parameters (such as phase fractions or c/a ratios), and electromechanical response is not systematically established in this study, this decline is phenomenologically consistent with the transition toward an average pseudo-cubic lattice with reduced macroscopic anisotropy.

As evidenced in Fig. S18, high donor concentrations substantially increase nucleation density and grain impingement, thereby suppressing extensive grain growth and producing fine-grained microstructures. Concurrent stabilization of pseudo-cubic symmetry progressively destabilizes long-range ferroelectric distortion, intrinsically reducing spontaneous polarization and electromechanical anisotropy. Thus, while the shift toward pseudo-cubic symmetry is indispensable for suppressing optical scattering, it simultaneously imposes a fundamental constraint on the macroscopic piezoelectric performance of KNN-based systems. These limitations indicate that achieving simultaneous optical transparency and strong electromechanical coupling is intrinsically difficult within donor-modified KNN systems. Accordingly, it is necessary to consider alternative perovskite systems that offer greater flexibility in phase stability and microstructural development.

In this regard, PZT-based systems provide a fundamentally different crystallographic and kinetic environment. Compared with KNN, PZT generally exhibits lower interfacial anisotropy, less faceted grain morphology, and more isotropic grain-growth behavior, collectively favoring the formation of coarse-grained dense microstructures. Furthermore, the well-established phase instability near the morphotropic phase boundary enables highly sensitive crystallographic tuning through donor incorporation.

Based on these considerations, the donor-mediated transparency strategy was extended to PZT using La^{3+} as a representative donor dopant. Due to the robust stability of ferroic distortion in PZT, significantly higher donor concentrations are necessitated to drive the pseudo-cubic transformation compared to KNN-based systems. Nevertheless, the fundamental mechanism remains identical: donor incorporation destabilizes symmetry-lowered ferroic states while simultaneously promoting liquid-phase-assisted densification and pore filling. Collectively, these results establish donor-controlled structural transformation and liquid-phase-assisted ultradensification as generalizable design principles for transparent multifunctional perovskite piezoelectric oxides.

3.3. Donor-Controlled Defect Chemistry and Hierarchical Phase transition in Transparent PLZT Piezoceramics

To extend the donor-mediated transparency strategy into a fundamentally distinct inorganic chemical regime, La^{3+}-modified $Pb(Zr,Ti)O_3$ (PLZT) ceramics were systematically investigated over a narrow compositional interval of x = 8.4-9.0, encompassing the critical transition from a long-range ferroelectric rhombohedral state to a pseudo-cubic structural configuration, as summarized in Figs. 8-10 and S19-S24. This compositional region is particularly significant because it corresponds to a chemically frustrated structural regime in which ferroic ordering, polarization anisotropy, and crystallographic symmetry become highly sensitive to donor-controlled defect equilibria. Within this narrow phase space, subtle variations in donor concentration produce profound changes in electromechanical response, optical scattering behavior, and polarization thermodynamics.

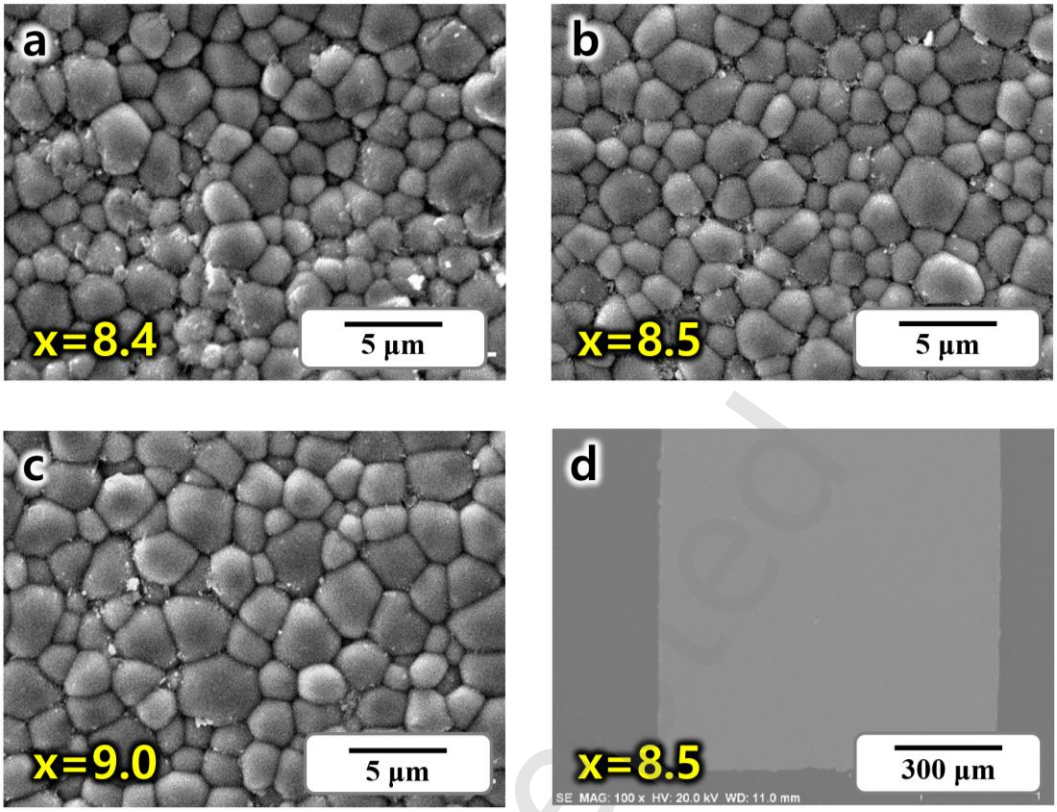

Fig. 8. SEM (SE) images of transparent PZT + x at.% La_2O_3 (8.4≤x≤9.0); a, x=8.4; **b** and **d**, x=8.5; **c**, x=9.0. Figure 8d is the SEM image of a polished specimen mounted with epoxy, while Figs. 5a-c are the SEM image of the surface of sintered specimens.

From an inorganic chemical standpoint, La^{3+} incorporation into the A-site of the ABO_3 perovskite lattice induces aliovalent substitution accompanied by charge-compensating defect formation. The replacement of Pb^{2+} by La^{3+} perturbs local charge neutrality and is compensated predominantly through the generation of A-site vacancies together with partial redistribution of oxygen vacancies. These defect equilibria substantially modify the local electrostatic environment surrounding the BO_6 octahedra, progressively weakening cooperative Pb-O off-centering and destabilizing long-range rhombohedral ferroelectric ordering. Consequently, the crystallographic free-energy landscape becomes increasingly flattened, reducing polarization anisotropy and continuously driving the system toward pseudo-cubic symmetry.

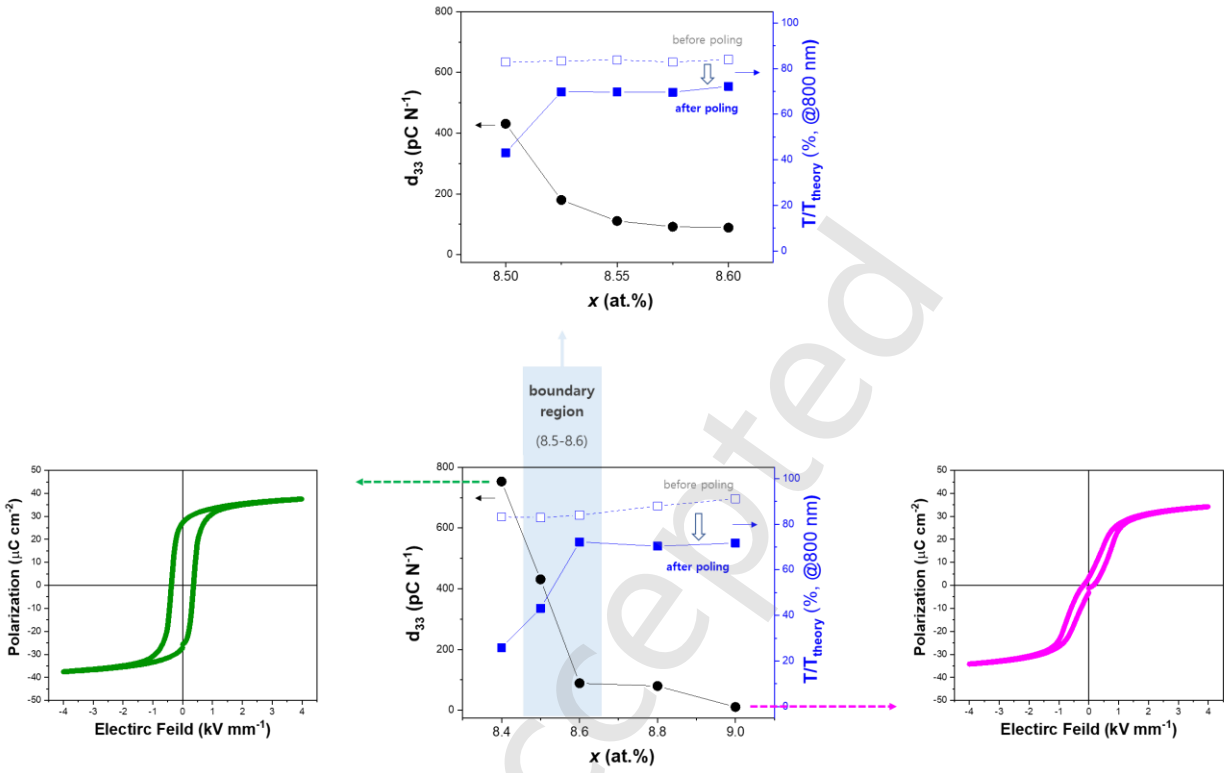

Fig. 9. Compositional variations in electromechanical and ferroelectric responses of transparent PZT + *x* at.% La_2O_3 ceramics (8.4 ≤ x ≤ 9.0, sample thickness: 1.0 mm**).** Representative polarization-electric field (*P*-*E*) hysteresis loops are shown for compositions on either side of the compositional boundary region, highlighting the change in ferroelectric switching behavior across this narrow interval. The accompanying plots summarize the corresponding piezoelectric/field-induced electromechanical characteristics together with the optical transmission/haze values at 630 nm, measured before and after poling, thereby elucidating the interplay among ferroelectric ordering, poling response, and optical transparency in the vicinity of the boundary composition.

Unlike KNN-based systems, PLZT exhibits intrinsically lower crystallographic and interfacial anisotropy owing to the comparatively isotropic bonding characteristics of the Pb-O-(Zr/Ti) framework. As shown in Figs. 8 and S19-S20, this manifests microstructurally as relatively coarse

equiaxed grains with sizes on the order of 2-5 μm, substantially larger than those observed in donor-modified KNN ceramics. Such behavior reflects fundamental differences in interfacial thermodynamics and grain-growth kinetics. Whereas KNN systems are dominated by highly faceted grain-boundary energetics associated with strong crystallographic anisotropy, PLZT is governed primarily by curvature-driven grain-boundary migration with comparatively isotropic interfacial energies. Consequently, PLZT sustains continuous grain coarsening even during rapid densification, producing highly dense microstructures with reduced intergranular scattering.

It is worth noting that the liquid-phase-assisted densification in the PLZT system is intrinsically governed by its defect chemistry. When considering the stoichiometry of $[(Pb_{1-x}La_x)(Zr,Ti)O_3]$, charge compensation through the coexistence of A-site and B-site vacancies inherently yields a slight local excess of PbO. At the sintering temperature of 1200 °C, this slight excess of PbO leads to the formation of a trace amount of transient liquid phase [48]. This microstructural liquid phase significantly expedites the densification process by promoting particle rearrangement and capillary-driven mass transport, which cooperatively facilitates the observed grain growth and pore elimination.

Structurally, the donor-induced rhombohedral-to-pseudo-cubic transformation in PLZT cannot be precisely characterized by diffraction analysis alone. As shown in Fig. S21b, the structural transition involves extremely subtle lattice distortions and minimal peak splitting, reflecting the near degeneracy of the competing crystallographic states. Because the average symmetry of the rhombohedral and pseudo-cubic phases remains highly similar, the principal distinction arises predominantly from local polar displacements rather than from large-scale periodic structural distortions.

To more directly probe this hidden structural transformation, polarization-electric field (P-E) hysteresis analysis was utilized as a sensitive probe of the ferroelectric free-energy landscape. As shown in Figs. 9 and S21a, compositions with $x \leq 8.5$ exhibit well-defined ferroelectric hysteresis loops characterized by substantial remanent polarization and coercive field, indicative of robust long-range Pb off-centering and stable rhombohedral ferroic order. In contrast, compositions approaching $x = 9.0$ progressively exhibit slim or nearly linear P-E behavior, consistent with collapse of the ferroelectric double-well potential into a weakly polar pseudo-cubic energy state. This continuous transformation is qualitatively consistent with a transition toward a weakly polar state, which conceptually points to a flattening of the energy barriers, driven by the progressive disruption of cooperative dipolar ordering around Pb-centered polar units.

The piezoelectric response evolves concomitantly with this structural transformation. As summarized in Fig. 9, the d_{33} value decreases sharply from 753 pC N^{-1} at $x = 8.4$ to 11 pC N^{-1} at $x = 9.0$. While the precise structural origin and quantitative phase-fraction contributions to this electromechanical decline require further systematic investigation, this sharp decrease qualitatively reflects the progressive suppression of ferroelastic switching pathways as average pseudo-cubic symmetry becomes stabilized. Simultaneously, optical transparency increases because donor-mediated reduction of polarization anisotropy suppresses birefringence-induced light scattering.

Importantly, a narrow compositional interval near $x = 8.5$-8.6 emerges as a structurally heterogeneous coexistence regime in which rhombohedral and pseudo-cubic characteristics persist simultaneously across multiple length scales. Within this regime, local polar nanoregions remain embedded within an average pseudo-cubic matrix, thereby generating a hierarchical polarization landscape stabilized by competing defect equilibria associated with La^{3+} incorporation. Such

structural heterogeneity prevents complete suppression of local polar ordering while sufficiently reducing long-range crystallographic anisotropy to minimize optical scattering.

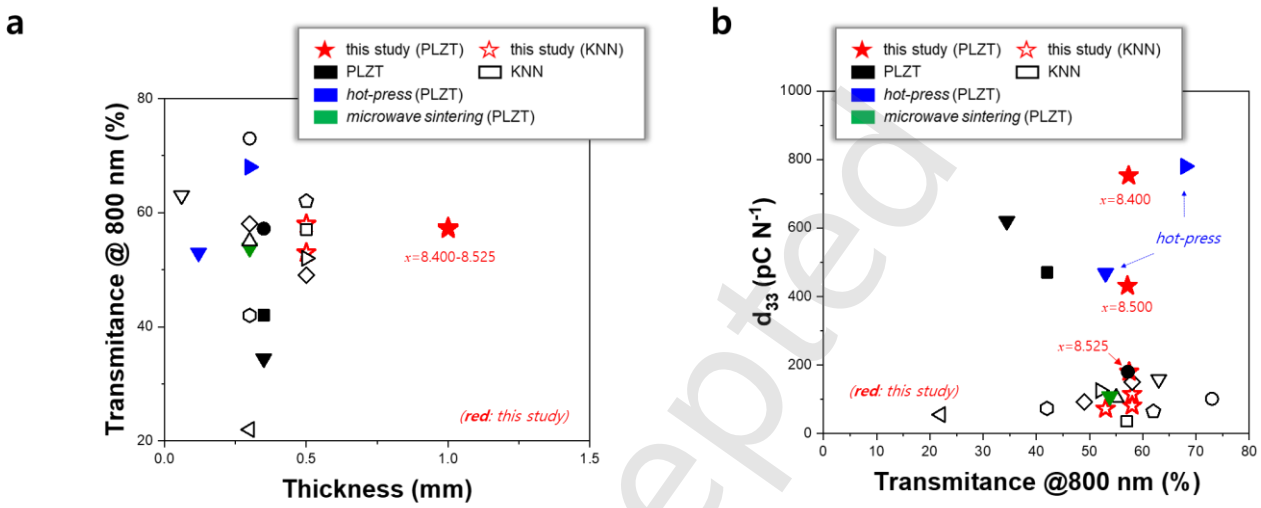

Fig. 10. Comparative performance maps of transparent piezoelectric materials (sample thickness of KNN: 0.5 mm, sample thickness of PLZT: 1.0 mm) [42-44,49-59]**.**

a, Optical transmittance at 800 nm plotted as a function of specimen thickness for various transparent piezoelectric materials reported in the literature.

b, Piezoelectric coefficient, d_{33}, plotted against optical transmittance, highlighting the trade-off between optical transparency and piezoelectric functionality. The red symbols denote the samples developed in this study, whereas the remaining symbols represent literature data for PLZT [$(Pb_{1-x}La_x)(Zr,Ti)O_3$]-, KNN-, and other transparent piezoelectric ceramics, including materials processed by hot pressing and microwave sintering. These comparisons show that the present materials occupy a highly competitive region of the property space, exhibiting an attractive balance between high optical transparency and substantial piezoelectric response.

As a consequence, compositions such as x = 8.525 and 8.6 simultaneously exhibit substantial piezoelectric coefficients of 431 and 180 pC N^{-1} together with high optical transparency. This unusual coexistence of electromechanical functionality and transparency originates from decoupling

between local and average structural symmetry: local Pb off-centering preserves electromechanical activity, whereas the averaged pseudo-cubic symmetry suppresses birefringence-induced optical scattering.

Microstructurally, the relatively coarse-grained nature of PLZT further contributes to enhanced electromechanical performance. Reduced grain-boundary density minimizes interfacial pinning of ferroelectric domain walls, thereby facilitating domain-wall mobility under external electric fields. In contrast to KNN-based systems, where donor-induced grain refinement imposes strong extrinsic constraints on domain switching, PLZT accommodates more fully developed ferroic domain structures within large grains, enabling efficient electromechanical coupling.

To systematically understand this disparity, the piezoelectric performance can be plausibly decoupled into intrinsic and extrinsic contributions. Intrinsically, the strong covalent Pb-O hybridization in PLZT is expected to preserve local polar displacements (local Pb off-centering) within the nanodomains even under an average pseudo-cubic symmetry. By contrast, in the KNN system, Bi^{3+} substitution likely destabilizes the polar anisotropy of the alkali-site framework, plausibly suppressing the intrinsic spontaneous polarization. Extrinsically, the stark contrast in grain size is highly likely to play a decisive role. While donor-doped KNN suffers from severe grain refinement (typically <1 μm) that is expected to pin the domain walls, PLZT maintains coarse grains (2-5 μm) with a low grain-boundary density. This microstructural difference is highly likely to preserve high domain-wall mobility and facilitate domain switching under external fields. Therefore, it is reasonable to view the retention of a much higher macroscopic d_{33} in transparent PLZT as a consequence of these cooperative factors.

Optically, transparency is governed by the simultaneous suppression of crystallographic and microstructural scattering sources. As shown in Figs. 9 and S22-S24, the pseudo-cubic x = 9.0 composition achieves a transmittance of approximately 72% at 800 nm (T/Ttheory = 68.9%, n = 2.5). This high transparency originates from the combined elimination of birefringence-induced scattering and reduced interfacial scattering within the coarse-grained dense microstructure.

A key outcome of the PLZT system is the breakdown of the conventional inverse relationship between optical transparency and piezoelectric activity. Recent studies on transparent KNN-based ceramics have demonstrated that the transparency-piezoelectricity trade-off can be mitigated through the deliberate engineering of local polarization configurations and multiscale structural heterogeneity [60-61]. In particular, controlling the coexistence of high-symmetry average structures and local polar regions provides an effective route to preserve electromechanical activity while suppressing optical scattering. These findings are consistent with the present results, where donor-controlled phase instability in PLZT enables the coexistence of an average pseudo-cubic structure and local polar activity near the rhombohedral-pseudo-cubic boundary.

As illustrated in Fig. 10, the present PLZT compositions simultaneously achieve high optical transmittance and substantial piezoelectric coefficients, surpassing the conventional trade-off behavior commonly observed in both transparent KNN ceramics and previously reported transparent PLZT systems. This enhanced multifunctionality originates from donor-controlled phase instability, interfacial isotropy, and hierarchical polarization coexistence governed by defect chemistry.

Overall, these results demonstrate that transparent piezoelectric functionality in PLZT originates not merely from average crystallographic symmetry control, but from a deeper inorganic chemical interplay among defect equilibria, polarization thermodynamics, interfacial energetics, and

hierarchical structural heterogeneity. More broadly, the present results establish donor-induced phase and defect modulation as a chemically generalizable strategy for designing multifunctional transparent perovskite piezoelectric oxides with simultaneously optimized optical and electromechanical properties.

4. Conclusions

This study demonstrates that the transformation of conventional piezoelectric ceramics into transparent materials via donor incorporation is dictated by interrelated inorganic chemical processes, including defect thermodynamics, crystallographic phase equilibria, and interfacial reaction kinetics. During donor-induced optical clarification, aliovalent doping systematically modulates cation-vacancy equilibria, local electrostatic potentials, and octahedral distortion energetics within the ABO_3 lattice. This conceptually links the defect equilibria with structural modifications, enabling the simultaneous orchestration of phase stability, ferroic anisotropy, densification behavior, and optical response in KNN- and PLZT-based systems.

Within this framework, transparent piezoelectric behavior in both KNN and PLZT systems is qualitatively described by the destabilization of long-range ferroic order in favor of nanoscale structural heterogeneity, wherein long-range ferroic order is progressively destabilized in favor of nanoscale structural heterogeneity. This transition enables a continuous evolution toward pseudo-cubic symmetry, effectively suppressing birefringence-driven scattering while preserving local polar non-centrosymmetry for electromechanical functionality. These findings define a fundamental inorganic chemical origin of transparency in ferroelectric perovskites.

In KNN-based systems, donor-induced phase instability coupled with liquid-phase-mediated densification promotes the elimination of residual porosity, yielding highly dense transparent ceramics.

In contrast, PLZT exhibits lower crystallographic anisotropy and more isotropic interfacial energetics, facilitating sustained grain coarsening and the development of dense transparent microstructures. Despite these divergent pathways, both systems are governed by defect-chemical modulation of interfacial thermodynamics, establishing a direct mechanistic link between atomic-scale defect processes and macroscopic optical transparency.

Accordingly, donor-mediated coordination of defect chemistry represents a generalizable inorganic chemical design concept for realizing transparent piezoelectric ceramics across diverse perovskite systems. Crucially, this paradigm allows researchers to retain their established piezoelectric compositions without abandonment or fundamental redesign; instead, transparent functionality can be directly induced by modulating the donor concentration in accordance with the intrinsic crystallographic stability of each host lattice. This shifts the focus from exploring entirely new material systems to re-functionalizing proven ones through precise defect control. While the present study focuses on establishing the defect-chemical origin of optical transparency using total transmittance as the principal optical metric, a comprehensive optimization of haze and in-line transmittance for high-resolution imaging and display applications is formally deferred to future systematic studies. Overall, this study establishes a unified defect-chemical and thermodynamic framework for transparent piezoelectric perovskites, in which optical transparency and electromechanical functionality are synergistically integrated through controlled manipulation of the free-energy landscape.

CRediT authorship contribution statement

S.-J.H, Y.K.M., J.-J.C, B.-D.H, H.-C.S., S.N., K.-H.C, and C.-W.A. conceptualized this study. **S.-J.H, S.-H. C., I.-R.Y., H.-A.C., J.-J.C., H.-C.S., S.N., K.-H.C., D.-C. A., and C.-W.A.** developed the methodology. **S.-J.H., H.-A.C., J.-J.C., K.-H.C., B.-J. M., D.-C. A., and C.-W.A.** performed the investigation. **S.-J.H., Y.K.M., H.-A.C., J.-J.C., B.-J. M., D.-C. A., and C.-W.A.** visualized the data.

J.-J.C., B.-D.H., and C.-W.A. acquired funding. **B.-D.H., H.-C.S., K.-H.C., and C.-W.A.** administered the project. **J.-J.C., B.-D.H., H.-C.S., K.-H.C., C.-W.A.** supervised the research. **S.-J.H., J.-J.C., B.-D.H., H.-C.S., K.-H.C. and C.-W.A.** wrote the original draft. **C.-W.A.** reviewed and edited the manuscript with input from all authors. All authors approved the final manuscript.

Declaration of competing interest

The authors declare that they have no known competing financial interests or personal relationships that could have appeared to influence the work reported in this paper.

Acknowledgements

This research was supported by the Nano & Material Technology Development Program through the National Research Foundation of Korea (NRF) funded by Ministry of Science and ICT (RS-2026-25586076) and the Fundamental Research Program of the Korea Institute of Materials Science (KIMS), "Development of next-generation multifunctional-materials for breakthrough in thermal management" (Grant No. PNKA890).

Availability of data and materials

The data that support the findings of this study are available from the corresponding author upon reasonable request.

Electronic Supplementary Material

Supplementary material is available in the online version of this article at https://doi.org/

References

[1] Curie P, Curie J. Development by stimulation of polarized bodies. *C R Acad Sci Paris* 1880, **91**: 294-295.

[2] Shirane G, Takeda A. Study of phase transitions in perovskite-type crystals. *J Phys Soc Jpn* 1952, **7**: 5-11.

[3] Egerton L, Dillon DM. Electron diffraction studies of phase transitions in ferroelectric ceramics. *J Am Ceram Soc* 1959, **42**: 438-442.

[4] Bai Y, Jantunen H, Juuti J. Energy harvesting research: The road from single source to multisource. *Adv Mater* 2018, **30**: 1707271.

[5] Dong L, Ke Y, Wang J, et al. Rational modeling and design of piezoelectric biomolecular thin films toward enhanced energy harvesting and sensing. *Adv Funct Mater* 2024, **34**: 2410566.

[6] Gao Z, Zhou Y, Zhang J, et al. Advanced energy harvesters and energy storage for powering wearable and implantable medical devices. *Adv Mater* 2024, **36**: 2404492.

[7] Hinchet R, Yoon HJ, Ryu H, et al. Transcutaneous ultrasound energy harvesting using capacitive triboelectric technology. *Science* 2019, **365**: 491-494.

[8] Li Z, Roscow J, Khanbareh H, et al. Energy harvesting from water flow by using piezoelectric materials. *Adv Energy Sustain Res* 2024, **5**: 2300235.

[9] Persano L, Camposeo A, Matino F, et al. Advanced materials for energy harvesting and soft robotics: Emerging frontiers to enhance piezoelectric performance and functionality. *Adv Mater* 2024, **36**: 2405363.

[10] Ren Z, Deng S, Shao J, et al. Ultrahigh-power-density flexible piezoelectric energy harvester based on freestanding ferroelectric oxide thin films. *Nat Commun* 2025, **16**: 3192.

[11] Han J, Park SH, Jung YS, et al. High-performance piezoelectric energy harvesting in amorphous perovskite thin films deposited directly on a plastic substrate. *Nat Commun* 2024, **15**: 4129.

[12] Zhang C, Jiang Z, Sun M, et al. Nature-inspired helical piezoelectric hydrogels for energy harvesting and self-powered human-machine interfaces. *Nano Energy* 2025, **110**: 110755.

[13] Li J, Rogan RC, Üstündag E, et al. Domain switching in polycrystalline ferroelectric ceramics. *Nat Mater* 2005, **4**: 776-781.

[14] Narayan B, Malhotra JS, Pandey R, et al. Electrostrain in excess of 1% in polycrystalline piezoelectrics. *Nat Mater* 2018, **17**: 427-431.

[15] Zhang MH, Shen C, Zhao C, et al. Deciphering the phase transition-induced ultrahigh piezoresponse in (K,Na)NbO_3-based piezoceramics. *Nat Commun* 2022, **13**: 3434.

[16] Wu W, Wang ZL. Piezotronics and piezo-phototronics for adaptive electronics and optoelectronics. *Nat Rev Mater* 2016, **1**: 16031.

[17] Fisher JG, Benčan A, Holc J, et al. Growth of potassium sodium niobate single crystals by solid state crystal growth. *J Cryst Growth* 2007, **303**: 487-492.

[18] Ahn CW, Lee HY, Han G, et al. Self-growth of centimeter-scale single crystals by normal sintering process in modified potassium sodium niobate ceramics. *Sci Rep* 2015, **5**: 17656.

[19] Ito H, Muromoto M, Kurenuma S, et al. Mechanical stimulation and solid seeding trigger single-crystal-to-single-crystal molecular domino transformations. *Nat Commun* 2013, **4**: 2009.

[20] Farooq MU, Fisher JG. Growth of ($K_{0.5}Na_{0.5}$)NbO_3-$SrTiO_3$ lead-free piezoelectric single crystals by the solid state crystal growth method and their characterization. *Ceram Int* 2014, **40**: 3199-3205.

[21] Kabakov P, Dean C, Kurusingal V, et al. Solid-state crystal growth of lead-free ferroelectrics. *J Mater Chem C* 2020, **8**: 7606-7615.

[22] Ahn CW, Park HW, Nahm S, et al. Structural variation and piezoelectric properties of 0.95($Na_{0.5}K_{0.5}$)NbO_3-0.05$BaTiO_3$ ceramics. *Sens Actuators A Phys* 2007, **136**: 255-260.

[23] Ahn CW, Park CS, Choi CH, et al. Sintering behavior of lead-free (K,Na)NbO_3-based piezoelectric ceramics. *J Am Ceram Soc* 2009, **92**: 2033-2038.

[24] Ahn CW, Choi CH, Park HY, et al. Dielectric and piezoelectric properties of (1-x)($Na_{0.5}K_{0.5}$)NbO_3-x$BaTiO_3$ ceramics. *J Mater Sci* 2008, **43**: 6784-6789.

[25] Ahn CW, Park CS, Priya S. Sintered composite for low temperature coefficient of piezoelectric property in KNN-based lead-free ceramics. *Funct Mater Lett* 2010, **3**: 35-38.

[26] Lin J, Wang Y, Xiong R, et al. Tailoring microstructure of eco-friendly temperature-insensitive transparent ceramics achieving superior piezoelectricity. *Acta Mater* 2022, **228**: 118061.

[27] Qiu C, Wang B, Zhang N, et al. Transparent ferroelectric crystals with ultrahigh piezoelectricity. *Nature* 2020, **577**: 350-354.

[28] Li C, Huan Y, Wang X, et al. Amelioration on energy storage performance of KNN-based transparent ceramics by optimizing the polarization and breakdown strength. *J Am Ceram Soc* 2022, **105**: 6158-6167.

[29] Hussain A, Ahn CW, Ullah A, et al. Dielectric, ferroelectric and field-induced strain behavior of $K_{0.5}Na_{0.5}NbO_3$-modified $Bi_{0.5}(Na_{0.78}K_{0.22})_{0.5}TiO_3$ lead-free ceramics. *Ceram Int* 2012, **38**: 4143-4148.

[30] Aissa M, Zannen M, Benyoussef M, et al. Large direct and inverse electrocaloric effects in lead-free Dy-doped 0.975KNN-0.025NBT ceramics. *Ceram Int* 2021, **47**: 31286-31294.

[31] Benedek G, Boscolo I, Handerek J, et al. Electron emission from ferroelectric/antiferroelectric cathodes excited by short high-voltage pulses. *J Appl Phys* 1997, **81**: 1396-1401.

[32] Ha SJ, Moon YK, Cha HA, et al. Fundamental study to grow single crystals with high performances operated up to high temperatures in donor-doped materials for energy harvesting. *Acta Mater* 2025, **295**: 121180.

[33] Tian H, Meng X, Hu C, et al. Origin of giant piezoelectric effect in lead-free $K_{1-x}Na_xTa_{1-y}Nb_yO_3$ single crystals. *Sci Rep* 2016, **6**: 25637.

[34] Peng L, Gao X, Liu X, et al. Synergism optimization of ferroelectric phase-transition temperature and piezoelectric properties of KNN-based ceramics by chemical composition regulation. *Mater Today Commun* 2024, **38**: 108214.

[35] Zuo R, Fang X, Ye C. Phase structures and electrical properties of new lead-free $(Na_{0.5}K_{0.5})NbO_3$-$(Bi_{0.5}Na_{0.5})TiO_3$ ceramics. *Appl Phys Lett* 2007, **90**: 092904.

[36] Choi SY, Yoon DY, Kang SJL. Kinetic formation and thickening of intergranular amorphous films at grain boundaries in barium titanate. *Acta Mater* 2004, **52**: 3721-3728.

[37] Wu W, Kadar A, Lee SH, et al. Layer-by-layer assembled nanowire networks enable graph-theoretical design of multifunctional coatings. *Matter* 2025, **8**: 101870.

[38] Chang Y, Ning H, Wu J, et al. Formation mechanism of (001)-oriented perovskite $SrTiO_3$ microplatelets synthesized by topochemical microcrystal conversion. *Inorg Chem* 2014, **53**: 11060-11066.

[39] Kang F, Yao B, Zhang W, et al. In situ topochemically converted 2D $BaTiO_3$ polycrystals with multifarious zone axes. *Mater Adv* 2022, **3**: 4878-4885.

[40] Poterala SF, Meyer RJ, Messing GL. Low-field dynamic magnetic alignment and templated grain growth of diamagnetic PMN-PT ceramics. *J Mater Res* 2013, **28**: 2960-2969.

[41] Haertling GH. PLZT electrooptic materials and applications–a review. *Ferroelectrics* 1987, **75**: 25-55.

[42] Lee Y, Choi H, Jang J. Fabrication and characterization of lead lanthanum zirconate titanate ceramic-based fully transparent piezoelectric loudspeakers for next-generation electronic devices. *Sens Actuators A Phys* 2025, **377**: 116087.

[43] Huang C, Xu J, Fang Z, et al. Effect of preparation process on properties of PLZT (9/65/35) transparent ceramics. *J Alloys Compd* 2017, **723**: 602-610.

[44] Yin QR, Ding AL, Zheng XS, et al. Preparation and characterization of transparent PZN-PLZT ceramics. *J Mater Res* 2004, **19**: 729-732.

[45] Ahn CW, Park CS, Dittmer R, et al. Effect of elemental diffusion on temperature coefficient of piezoelectric properties in KNN-based lead-free composites. *J Mater Sci* 2010, **45**: 3961-3966.

[46] Liao J, Lv X, Sun X, et al. Boosting piezocatalytic activity of KNN-based materials with phase boundary and defect engineering. *Adv Funct Mater* 2023, **33**: 2303637.

[47] Cen Z, Bian S, Xu Z, et al. Simultaneously improving piezoelectric properties and temperature stability of $Na_{0.5}K_{0.5}NbO_3$-based ceramics sintered in reducing atmosphere. *J Adv Ceram* 2021, **10**: 820-829.

[48] Choi JJ, Ryu J, Kim HE. Microstructural evolution of transparent PLZT Ceramics Sintered in Air and Oxygen Atmospheres. *J Am Ceram Soc* 2001, **84**: 1465-1469.

[49] Chu K, Shi Y, Li K, et al. Design of high performance lead-free (K,Na)NbO_3-based piezoelectric ceramics. *J Phys Chem Solids* 2015, **81**: 10-14.

[50] Kwok KW, Li F, Lin D. A novel lead-free transparent ceramic with high electro-optic coefficient. *Funct Mater Lett* 2011, **4**: 237-240.

[51] Li D, Gu W, Irshad MS, et al. Simultaneously achieving high transparency and applicable piezoelectricity in Sm-modified KNN-based lead-free ceramics. *J Alloys Compd* 2023, **955**: 170209.

[52] Rahman A, Jiang M, Rao G, et al. Improved ferroelectric, piezoelectric, and dielectric properties in pure KNN translucent ceramics by optimizing the normal sintering method. *Ceram Int* 2022, **48**: 20251-20259.

[53] Rahman A, Park S, Min Y, et al. An easy approach to obtain large piezoelectric constant in high-quality transparent ceramics by normal sintering process in modified potassium sodium niobate ceramics. *J Eur Ceram Soc* 2020, **40**: 2989-2996.

[54] Ren X, Peng Z, Chen B, et al. A compromise between piezoelectricity and transparency in KNN-based ceramics: The dual functions of Li_2O addition. *J Eur Ceram Soc* 2020, **40**: 2331-2337.

[55] Wu X, Lu S, Kwok KW. Photoluminescence, electro-optic response and piezoelectric properties in pressureless-sintered Er-doped KNN-based transparent ceramics. *J Alloys Compd* 2017, **695**: 3573-3578.

[56] Yang D, Ma C, Yang Z, et al. Optical and electrical properties of pressureless sintered transparent $(K_{0.37}Na_{0.63})NbO_3$-based ceramics. *Ceram Int* 2016, **42**: 4648-4654.

[57] Zhang X, Yang D, Yang Z, et al. Transparency of $K_{0.5}Na_{0.5}NbO_3$-$Sr(Mg_{1/3}Nb_{2/3})O_3$ lead-free ceramics modulated by relaxor behavior and grain size. *Ceram Int* 2016, **42**: 17963-17971.

[58] Zhao X, Chai Q, Chen B, et al. Improved transmittance and ferroelectric properties realized in KNN ceramics via SAN modification. *J Am Ceram Soc* 2018, **101**: 5127-5137.

[59] Zhao X, Chao X, Wu D, et al. Simultaneous realization of high transparency and piezoelectricity in low symmetry KNN-based ceramics. *J Am Ceram Soc* 2019, **102**: 3498-3509.

[60] Lin Q, Shen J, Zeng X, et al. Breaking the transparency-piezoelectricity trade-off in lead-free ceramics via tailoring local polarization configuration. *ACS Nano* 2026, **20**: 17803-17818.

[61] Lin Q, Zeng X, Huang X, et al. Multiscale reconfiguration achieving high electromechanical performance in $K_{0.5}Na_{0.5}NbO_3$-based transparent ceramics for pressure-warning smart window. *Chem Eng J* 2025, **520**: 165886.

Graphical abstract